

The fractional symmetric rigid rotor

Richard Herrmann ^a

GigaHedron, Farnweg 71, D-63225 Langen, Germany

Received: September 15, 2006 / Revised version: February 9, 2008

Abstract. Based on the Riemann fractional derivative the Casimir operators and multiplets for the fractional extension of the rotation group $SO(n)$ are calculated algebraically. The spectrum of the corresponding fractional symmetric rigid rotor is discussed. It is shown, that the rotational, vibrational and γ -unstable limits of the standard geometric collective models are particular limits of this spectrum. A comparison with the ground state band spectra of nuclei shows an agreement with experimental data better than 2%. The derived results indicate, that the fractional symmetric rigid rotor is an appropriate tool for a description of low energy nuclear excitations.

PACS. 21.60.Fw Group theory nuclear physics – 21.10.k Nuclear energy levels

1 Introduction

The concept of fractional calculus has inspired mathematicians since the days of Leibniz[?]-[2].

In physics, early attempts to use this concept in the field of applications had been studies on non-local dynamics, e.g. anomalous diffusion or fractional Brownian motion [3],[4].

During the last decade, remarkable progress has been made in the theory of fractional wave equations[5]-[8]. But until now, there exists no application of the fractional calculus in nuclear theory.

We therefore will first introduce the necessary tools for a fractional extension of the standard definition of angular momentum operators, derive the Casimir operators and classify the multiplets of a fractional extension of the standard rotation group $SO(n)$.

We will then discuss the properties of the corresponding fractional symmetric rigid rotor spectrum and the results of its application to the low energy excitation ground state band spectra of even-even nuclei.

2 Fractional quantum mechanical observables

The transition from classical mechanics to quantum mechanics may be performed by canonical quantisation [9], [10]. The classical canonically conjugated observables x and p are replaced by quantum mechanical observables \hat{X} and \hat{P} , which are introduced as derivative operators on a Hilbert space of square integrable wave functions f . The space coordinate representations of these operators are

$$\hat{X}f(x) = xf(x) \quad (1)$$

$$\hat{P}f(x) = -i\hbar\partial_x f(x) \quad (2)$$

where \hat{X} and \hat{P} fulfill the commutation relation

$$[\hat{X}, \hat{P}] = i\hbar \quad (3)$$

We will now describe a generalisation of these operators from integer order derivative to arbitrary order derivative.

The definition of the fractional order derivative is not unique, several definitions e.g. the Caputo, Weyl, Riesz, Grünwald [11]-[14] fractional derivative definition coexist. For our purpose, we apply as a specific representation of the fractional derivative operator the widely used Riemann-Liouville fractional derivative [15] of order α , where α is a real number in the interval $[0, 1]$:

$$D_x^\alpha(x)f(x) = \frac{1}{\Gamma(1-\alpha)} \frac{\partial}{\partial x} \int_0^x d\xi (x-\xi)^{-\alpha} f(\xi) \quad (4)$$

Since (4) is valid for $x > 0$ only, we define the variable $\bar{\chi}$ and the corresponding fractional derivative $\bar{D}_{\bar{\chi}}$ as:

$$\bar{\chi} = \text{sign}(x) |x|^\alpha \quad (5)$$

$$\bar{D}_{\bar{\chi}} = \text{sign}(x) D_x^\alpha(|x|) \quad (6)$$

With the definitions (4)-(6) we are able to calculate fractional derivatives for real numbers R , e.g. for $f(\bar{\chi}) = \bar{\chi}^\nu$ we obtain:

$$\bar{D}_{\bar{\chi}} \bar{\chi}^\nu = \frac{\Gamma(1+\nu\alpha)}{\Gamma(1+(\nu-1)\alpha)} \bar{\chi}^{\nu-1} \quad \nu\alpha > -1 \quad (7)$$

Furthermore, we are able to define Riemann-Taylor series $f(\bar{\chi})$ on R :

$$f(\bar{\chi}) = |\bar{\chi}|^{\frac{\alpha-1}{\alpha}} \sum_{n=0}^{\infty} a_n \bar{\chi}^n \quad (8)$$

^a email address: herrmann@gigahedron.com

To construct a Hilbert space with these functions $f(\bar{\chi})$ we use the Riemann-Liouville fractional integral [15] of order α :

$$I_x^\alpha(x)f(x) = \frac{1}{\Gamma(\alpha)} \int_0^x d\xi (x - \xi)^{\alpha-1} f(\xi) \quad (9)$$

Just like the Riemann-Liouville fractional derivative, this integral is valid for $x > 0$ only. Therefore, we define an integral operator on R :

$$\int_{-|x|}^{|x|} d\bar{u} = \text{sign}(x) I_x^\alpha(|x|) \quad (10)$$

The fractional scalar product is then given as:

$$\langle f|g \rangle = \int_{-|x|}^{|x|} d\bar{u} f^*(\bar{\chi}) g(\bar{\chi}) \quad (11)$$

With these definitions, the fractional quantum mechanical observables \hat{X} and \hat{P} finally read in space coordinate representation as:

$$\hat{X} f(\bar{\chi}) = \left(\frac{\hbar}{mc} \right)^{(1-\alpha)} \bar{\chi} f(\bar{\chi}) \quad (12)$$

$$\hat{P} f(\bar{\chi}) = -i \left(\frac{\hbar}{mc} \right)^\alpha mc \bar{D}_{\bar{\chi}} f(\bar{\chi}) \quad (13)$$

The attached factors $(\hbar/mc)^{(1-\alpha)}$ and $(\hbar/mc)^\alpha mc$ respectively ensure correct length and momentum units. For $\alpha = 1$ these definitions reduce to (1) and (2).

Since the Leibniz' product rule is not valid in its original form anymore for fractional derivatives [16], commutation relations depend on the specific choice of the function set, they are acting on. For a function set $\{f(\bar{\chi}) = \bar{\chi}^\nu\}$, using (7), the fractional conjugated operators satisfy the following commutation relation:

$$\begin{aligned} [\hat{X}, \hat{P}] &= -i\hbar \left(\frac{\Gamma(1+\nu\alpha)}{\Gamma(1+(\nu-1)\alpha)} - \frac{\Gamma(1+(\nu+1)\alpha)}{\Gamma(1+\nu\alpha)} \right) \\ &= -i\hbar c(\nu, \alpha) \end{aligned} \quad (14) \quad (15)$$

In (15) we have introduced $-i\hbar c(\nu, \alpha)$ as a short hand notation of the commutator. For $\alpha = 1$ this commutator is equivalent with (3).

The results derived so far may easily be extended to the multi dimensional case. For the Euclidean space of N particles we obtain the following sets of fractional conjugated operators in space coordinate representation:

$$\{\hat{X}_i\} = \left\{ \left(\frac{\hbar}{mc} \right)^{(1-\alpha)} \bar{\chi}_i \right\} \quad (16)$$

$$\{\hat{P}_i\} = \left\{ -i \left(\frac{\hbar}{mc} \right)^\alpha mc \bar{D}_i \right\} \quad i = 1, \dots, 3N \quad (17)$$

where we have introduced the abbreviation \bar{D}_i for $\bar{D}_{\bar{\chi}_i}$.

On a function set of the form $\{f(\bar{\chi}_1, \bar{\chi}_2, \dots, \bar{\chi}_{3N}) = \prod_i^{3N} \bar{\chi}_i^{\nu_i}\}$, the fractional conjugated operators satisfy the

following commutation relations:

$$[\hat{X}_i, \hat{X}_j] = 0 \quad (18)$$

$$[\hat{P}_i, \hat{P}_j] = 0 \quad (19)$$

$$\begin{aligned} [\hat{X}_i, \hat{P}_j] &= -i\hbar \delta_{ij} \left(\frac{\Gamma(1+\nu_i\alpha)}{\Gamma(1+(\nu_i-1)\alpha)} - \frac{\Gamma(1+(\nu_i+1)\alpha)}{\Gamma(1+\nu_i\alpha)} \right) \\ &= -i\hbar \delta_{ij} c(\nu_i, \alpha) \end{aligned} \quad (20) \quad (21)$$

With definitions (16),(17), we are now able to quantise classical operators, e.g. the classical angular momentum $L_{ij}^{\text{classical}} = x_i p_j - x_j p_i$ by use of the canonical quantisation procedure [9],[10].

3 Classification of angular momentum eigenstates

According to the results from the previous section, we define the generators of infinitesimal rotations in the i, j -plane ($i, j = 1, \dots, 3N$), with N being the number of particles):

$$\begin{aligned} L_{ij} &= \hat{X}_i \hat{P}_j - \hat{X}_j \hat{P}_i \\ &= -i\hbar (\bar{\chi}_i \bar{D}_j - \bar{\chi}_j \bar{D}_i) \end{aligned} \quad (22)$$

On a function set

$$\{f(\bar{\chi}_1, \bar{\chi}_2, \dots, \bar{\chi}_{3N}) = \prod_i^{3N} \bar{\chi}_i^{\nu_i}\} \quad (23)$$

the commutation relations for L_{ij} are isomorph to an extended fractional $SO^\alpha(3N)$ algebra:

$$[L_{ij}, L_{mn}] = i\hbar c(\nu, \alpha) (\delta_{im} L_{jn} + \delta_{jn} L_{im} - \delta_{in} L_{jm} - \delta_{jm} L_{in}) \quad (24)$$

Consequently, we can proceed in a standard way [18],[19]. We define a set of Casimir operators Λ_k^2 , where the index k indicates the Casimir operator associated with $SO^\alpha(k)$:

$$\Lambda_k^2 = \frac{1}{2} \sum_{i,j}^k (L_{ij})^2 \quad k = 2, \dots, 3N \quad (25)$$

which indeed fulfills the relations $[\Lambda_{3N}^2, L_{ij}] = 0$ and successively $[\Lambda_k^2, \Lambda_{k'}^2] = 0$. Therefore the multiplets of $SO^\alpha(3N)$ are classified according to the group chain

$$SO^\alpha(3N) \supset SO^\alpha(3N-1) \supset \dots \supset SO^\alpha(3) \supset SO^\alpha(2) \quad (26)$$

We use Einstein's summation convention and introduce the metric of the Euclidean space to be $g_{ij} = \delta_{ij}$ for raising and lowering indices. The explicit form of the Casimir operators is then given by

$$\begin{aligned} \Lambda_k^2 &= +\hat{X}^i \hat{X}_i \hat{P}^j \hat{P}_j - i\hbar c(\nu, \alpha) (k-1) \hat{X}^i \hat{P}_j - \hat{X}^i \hat{X}^j \hat{P}_i \hat{P}_j \\ &\quad i = 1, \dots, k \end{aligned} \quad (27)$$

The classical homogeneous Euler operator is defined as $x_1 \partial_{x_1} + x_2 \partial_{x_2} + \dots + x_k \partial_{x_k}$. We introduce a generalisation of the classical homogeneous Euler operator J_k^e for fractional derivative operators

$$J_k^e = \bar{\chi}^i \bar{D}_i \quad i = 1, \dots, k \quad (28)$$

With the generalised homogeneous Euler operator the Casimir operators are:

$$A_k^2 = +\hat{X}^i \hat{X}_i \hat{P}^j \hat{P}_j + \hbar^2 \left(c(\nu, \alpha) (k-2) J_k^e + J_k^e J_k^e \right) \quad i = 1, \dots, k \quad (29)$$

From this equation it follows, that the Casimir operator is diagonal on a function set f , if the generalised homogeneous Euler operator is diagonal on f and if f fulfills the Laplace-equation $\bar{D}^i \bar{D}_i f = 0$.

We will show, that the generalised homogeneous Euler operator is diagonal, if f fulfills an extended fractional homogeneity condition, which we will derive in the following. For that purpose, we first verify, that the generalised homogeneous Euler operator is diagonal on a homogeneous function in the one dimensional case.

We apply the following scaling property, which is valid for the fractional derivative [16], with $\bar{\lambda} = \text{sign}(\lambda) |\lambda|^\alpha$:

$$\bar{D}_{\bar{\lambda}} f(\bar{\lambda} \bar{\chi}) = \bar{\chi} \bar{D}_{\bar{\lambda} \bar{\chi}} f(\bar{\lambda} \bar{\chi}) \quad (30)$$

Homogeneity of a function in one dimension implies:

$$f(\bar{\lambda} \bar{\chi}) = \bar{\lambda}^\nu f(\bar{\chi}) \quad \nu > -1 \quad (31)$$

Applying the derivative operator $\bar{D}_{\bar{\lambda}}$ on (31), using (30) and (7) leads to:

$$\bar{\chi} \bar{D}_{\bar{\lambda} \bar{\chi}} f(\bar{\lambda} \bar{\chi}) = \frac{\Gamma(1 + \nu \alpha)}{\Gamma(1 + (\nu - 1) \alpha)} \bar{\lambda}^{\nu-1} f(\bar{\chi}) \quad (32)$$

Setting $\bar{\lambda} = 1$ reduces (32) to:

$$\bar{\chi} \bar{D}_{\bar{\chi}} f(\bar{\chi}) = \frac{\Gamma(1 + \nu \alpha)}{\Gamma(1 + (\nu - 1) \alpha)} f(\bar{\chi}) \quad (33)$$

The left hand side of (33) is nothing else but the generalised homogeneous Euler operator (28) in one dimension $J_{k=1}^e$.

Therefore, for the multi dimensional case, on a function set of the form

$$\{f(\bar{\chi}_1, \bar{\chi}_2, \dots, \bar{\chi}_k) = \sum_{\nu_i} a_{\nu_1 \nu_2 \dots \nu_k} \bar{\chi}_1^{\nu_1} \bar{\chi}_2^{\nu_2} \dots \bar{\chi}_k^{\nu_k}\} \quad (34)$$

the Euler operator J_k^e is diagonal, if the ν_i fulfill the following condition:

$$\sum_{i=1}^k \frac{\Gamma(1 + \nu_i \alpha)}{\Gamma(1 + (\nu_i - 1) \alpha)} = \frac{\Gamma(1 + \nu \alpha)}{\Gamma(1 + (\nu - 1) \alpha)} \quad (35)$$

This is the fractional homogeneity condition.

Hence we define the Hilbert space H^α of all functions f , which fulfill the fractional homogeneity condition (35),

satisfy the Laplace equation $\bar{D}^i \bar{D}_i f = 0$ and are normalised in the interval $[-1, 1]$.

We propose the quantisation condition:

$$\nu = n \quad n = 0, 1, 2, \dots \quad (36)$$

Where n is a non-negative integer. This specific choice reduces to the classical quantisation condition for the case $\alpha = 1$.

On this Hilbert space H^α , the generalised homogeneous Euler operator J_k^e is diagonal and has the eigenvalues $l_k(\alpha, n)$

$$l_k(\alpha, n) = \frac{\Gamma(1 + n \alpha)}{\Gamma(1 + (n - 1) \alpha)} \quad n = 0, 1, 2, \dots \quad (37)$$

The eigenvalues of the Casimir-operators on H^α follow as:

$$A_2 f = \hbar l_2(\alpha, n) f \quad (38)$$

$$A_k^2 f = \hbar^2 l_k(\alpha, n) \left(l_k(\alpha, n) + c(n, \alpha) (k - 2) \right) f \quad k = 3, \dots, N \quad (39)$$

with

$$l_k(\alpha, n) \geq l_{k-1}(\alpha, n) \geq \dots \geq | \pm l_2(\alpha, n) | \geq 0 \quad (40)$$

We have derived an analytic expression for the full spectrum of the Casimir operators for the $SO^\alpha(3N)$, which may be interpreted as a projection of function set (34) on to function set (23) determined by the fractional homogeneity condition (35).

For the special case of only one particle ($N = 1$), we can introduce the quantum numbers J and M , which now denote the J -th and M -th eigenvalue $l_3(\alpha, J)$ and $l_2(\alpha, M)$ of the generalised homogeneous Euler operators J_3^e and J_2^e respectively. The eigenfunctions are fully determined by these two quantum numbers $f = |JM\rangle$.

With the definitions $\hat{J}_z(\alpha) = A_2 = L_{12}$ and $\hat{J}^2(\alpha) = A_3^2 = L_{12}^2 + L_{13}^2 + L_{23}^2$ it follows

$$\hat{J}_z(\alpha) |JM\rangle = \hbar \frac{\Gamma(1 + M \alpha)}{\Gamma(1 + (M - 1) \alpha)} |JM\rangle \quad M = 0, \pm 1, \pm 2, \dots, \pm J \quad (41)$$

$$\hat{J}^2(\alpha) |JM\rangle = \hbar^2 \frac{\Gamma(1 + (J + 1) \alpha)}{\Gamma(1 + (J - 1) \alpha)} |JM\rangle \quad J = 0, +1, +2, \dots \quad (42)$$

For $\alpha = 1$ equations (41) and (42) reduce to

$$\hat{J}_z(\alpha = 1) |JM\rangle = \hbar M |JM\rangle \quad M = 0, \pm 1, \pm 2, \dots, \pm J \quad (43)$$

$$\hat{J}^2(\alpha = 1) |JM\rangle = \hbar^2 J(J + 1) |JM\rangle \quad J = 0, +1, +2, \dots \quad (44)$$

and $\hat{J}^2(\alpha = 1)$, $\hat{J}_z(\alpha = 1)$ reduce to the definitions of \hat{J}^2, \hat{J}_z used in standard quantum mechanical angular momentum algebra [20], [21].

The complete set of eigenvalues of a $SO^\alpha(3)$ multiplet is given by (41) and (42). Hence we are able to search for a realisation of $SO^\alpha(3)$ symmetry in nature. Promising candidates for a still unrevealed $SO^\alpha(3)$ symmetry are the ground state band spectra of even-even nuclei. Therefore we will introduce the fractional symmetric rigid rotor model in the next section and discuss some of its applications.

4 Eigenvalues of the fractional symmetric rigid rotor model

The fractional Schrödinger equation is given by (see [7])

$$H\Psi = E\Psi \quad (45)$$

The requirement of invariance under fractional rotations in R^3 completely determines the structure of the fractional Hamiltonian up to a constant factor A_0 :

$$H = m_0 + A_0 \Lambda_3^2(SO^\alpha(3)) \quad (46)$$

$$= m_0 + A_0 \hat{J}^2(\alpha) \quad (47)$$

where m_0 mainly acts as a counter term for the zero point energy contribution of the fractional rotational energy and A_0 is a measure for the level spacing.

On a function set $|JM\rangle$ the Hamiltonian is diagonal. Furthermore, due to definitions (5),(6) the Hamiltonian commutes with the parity operator Π , $[H, \Pi] = 0$.

For $\alpha = 1$ the function set $|JM\rangle$ reduces to the set of spherical harmonics Y_{JM} in cartesian representation. The eigenvalues of the parity operator Π are given by [27]

$$\begin{aligned} \Pi Y_{JM}(x_1, x_2, x_3) &= Y_{JM}(-x_1, -x_2, -x_3) \\ &= (-1)^J Y_{JM}(x_1, x_2, x_3) \end{aligned} \quad (48)$$

Therefore, the wave function is invariant under parity transformation Π , if J is restricted to even, non-negative integers $J = 0, 2, 4, \dots$. In a collective geometric model, this symmetry is interpreted as the geometry of the symmetric rigid rotor model [23].

Whether or not the behaviour (48) is still valid for the function set $|JM\rangle$ with arbitrary α cannot be proven directly with the methods developed so far.

Nevertheless, restricting J to be an even, non-negative integer $J = 0, 2, 4, \dots$ for arbitrary α , implies a symmetry, which we call in analogy to the case $\alpha = 1$ the fractional symmetric rigid rotor, even though this term lacks a direct geometric interpretation for $\alpha \neq 1$.

Hence we define the spectrum of a fractional symmetric rigid rotor:

$$E = E_J^\alpha = m_0 + A_0 \hbar^2 \frac{\Gamma(1 + (J+1)\alpha)}{\Gamma(1 + (J-1)\alpha)}, \quad J = 0, 2, 4, \dots \quad (49)$$

In figure 1 this energy spectrum is plotted for different values of α .

As a general trend the higher angular momentum energy values are decreasing for $\alpha < 1$. This behaviour is a well established observation for nuclear low energy rotational band structures [23].

In a classical geometric picture of the nucleus [22], [23] this phenomenon is interpreted as a change of the nuclear shape under rotations, causing an increasing moment of inertia. Now, with a fixed moment of inertia (A_0 is a constant) in our approach for the fractional rotational energy, the same effect results as an inherent property of the fractional derivatives angular momentum.

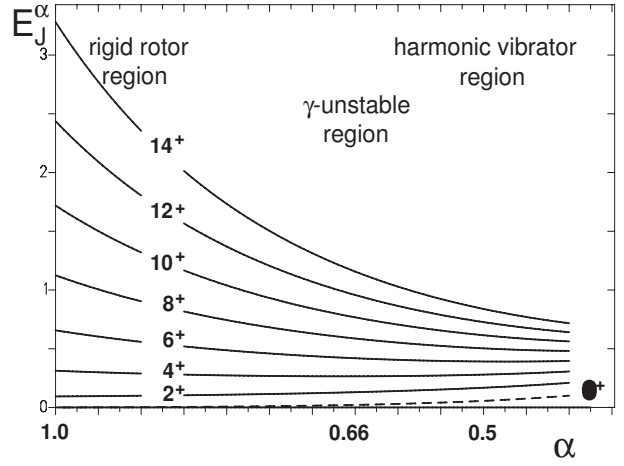


Fig. 1. energy spectrum E_J^α from (49) of the fractional symmetric rigid rotor

Another remarkable characteristic of the fractional symmetric rigid rotor spectrum is due to the fact, that the relative spacing between different levels is changing (see figure 2).

In classical geometric models there are distinct analytically solvable limits, e.g. the rotational, vibrational and so called γ -unstable limits [23].

These limits are characterised by their independence of the potential energy from γ . In that case, the five dimensional Bohr Hamiltonian is separable [22],[26]. With the collective coordinates β , γ and the three Euler angles θ_i the product ansatz for the wave function

$$\Psi(\beta, \gamma, \theta_i) = f(\beta)\Phi(\gamma, \theta_i) \quad (50)$$

leads to a differential equation for β , expressed in canonical form

$$\left\{ \frac{\hbar^2}{2B} \left(-\frac{\partial^2}{\partial \beta^2} + \frac{(\tau+1)(\tau+2)}{\beta^2} \right) + V(\beta) \right\} (\beta^2 f(\beta)) = E(n_\beta, \tau) (\beta^2 f(\beta)) \quad (51)$$

The ground state spectra of nuclei, based on γ independent potentials, are then determined by the conditions [26]:

$$\begin{aligned} n_\beta &= 0 \\ 2\tau &= J, \quad \tau = 0, 1, 2, \dots \end{aligned} \quad (52)$$

In the following we will prove, that the above mentioned limits are included within the fractional symmetric rigid rotor spectrum as special cases at distinct α -values. This is a further indication, that the fractional symmetric rigid rotor model may be successfully applied to low energy excitation spectra of nuclei.

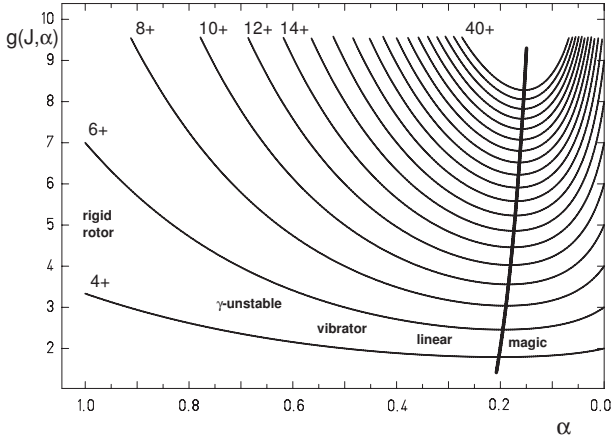


Fig. 2. relative energy levels $g(J, \alpha) = (E_J^\alpha - E_0^\alpha)/(E_2^\alpha - E_0^\alpha)$ with E_J^α from (49) of the fractional symmetric rigid rotor. The thick line shows the minimum achievable ratio for a given J as a function of α .

4.1 Rotational limit

In the geometric collective model the rotational limit is described by the symmetric rigid rotor [24],[23]:

$$E = \frac{1}{2} \frac{\hbar^2}{\Theta} J(J+1) \quad , \quad J = 0, 2, 4, \dots \quad (53)$$

This limit is trivially included in the fractional symmetric rigid rotor spectrum for $\alpha = 1$

$$\begin{aligned} E_J^{\alpha=1} &= m_0 + A_0 \hbar^2 \frac{\Gamma(1 + (J+1))}{\Gamma(1 + (J-1))} \\ &= m_0 + A_0 \hbar^2 \frac{(J+1)!}{(J-1)!} \\ &= m_0 + A_0 \hbar^2 J(J+1) \quad , \quad J = 0, 2, 4, \dots \end{aligned} \quad (54)$$

Setting $m_0 = 0$ and $A_0 = 1/(2\Theta)$ completes the derivation.

Remarkably enough, reading (54) backwards is an application of the original Euler concept for a fractional derivative, since Euler suggested a replacement of $n!$ for the discrete case by $\Gamma(1+z)$ for the fractional case [17].

4.2 Vibrational limit

In the geometric collective model the vibrational limit is described by a harmonic oscillator potential e. g. [23]

$$V(\beta) = \frac{1}{2} C \beta^2 \quad (55)$$

where C is the stiffness in β -direction. The level spectrum is given by

$$E = \hbar \omega (N + 5/2) \quad (56)$$

with $\omega = \sqrt{C/B}$ and

$$N = 2n_\beta + \tau \quad , \quad N = 0, 1, 2, 3, \dots \quad (57)$$

Therefore the ground state band $E^{g.s.}$ is given according to the conditions (52) by

$$E^{g.s.}(\tau) = \hbar \omega (\tau + 5/2) \quad \tau = 0, 1, 2, \dots \quad (58)$$

We will prove, that for $\alpha = 1/2$ the spectrum for the fractional symmetric rigid rotor corresponds to this vibrational type ground state spectrum

$$\begin{aligned} E_J^{\alpha=1/2} &= m_0 + A_0 \hbar^2 \frac{\Gamma(1 + \frac{1}{2}(J+1))}{\Gamma(1 + \frac{1}{2}(J-1))} \\ &= m_0 + A_0 \hbar^2 \frac{\Gamma(1 + J/2 + \frac{1}{2})}{\Gamma(1 + J/2 - \frac{1}{2})} \\ &= m_0 + A_0 \hbar^2 \frac{\Gamma(1 + J/2 + \frac{1}{2})}{\Gamma(J/2 + \frac{1}{2})} \\ &= m_0 + A_0 \hbar^2 (J/2 + \frac{1}{2}) \quad , \quad J = 0, 2, 4, \dots \end{aligned} \quad (59)$$

where we have used $\Gamma(1+z) = z\Gamma(z)$.

Since $J = 2\tau$ for the ground state band we get:

$$E_J^{\alpha=1/2} = m_0 + A_0 \hbar^2 (\tau + \frac{1}{2}) \quad , \quad \tau = 0, 1, 2, \dots \quad (60)$$

Setting $m_0 = 2\hbar\omega$ and $A_0 = \omega/\hbar$ completes the derivation.

The appearance of the correct equidistant level spacing including the zero point energy contribution of the harmonic oscillator eigenvalues is due to the fact, that the Riemann fractional derivative does not vanish when applied to a constant function.

Instead, for the fractional symmetric rigid rotor based on the Riemann fractional derivative there always exists a zero point energy for $\alpha \neq 1$ of the form

$$\hat{J}^2(\alpha) |00\rangle = \hbar^2 \frac{\Gamma(1+\alpha)}{\Gamma(1-\alpha)} |00\rangle \quad (61)$$

Hence the consistence with the spectrum of the harmonic oscillator including the zero point energy is a strong argument for our specific choice of the Riemann fractional derivative definition.

4.3 Davidson potential - the so called γ -unstable limit

There exists a third analytically solvable case, which is based on the Davidson potential [25], which originally was proposed to describe an interaction in diatomic molecules.

The potential is of the form

$$V(\beta) = \frac{1}{8} C \beta_0^2 \left(\frac{\beta}{\beta_0} - \frac{\beta_0}{\beta} \right)^2 \quad (62)$$

where β_0 (the position of the minimum) and C (the stiffness in β -direction at the minimum) are the parameters of the model.

For $\beta_0 = 0$ this potential is equivalent to the harmonic oscillator potential.

The energy level spectrum is given by

$$E(n_\beta, \tau) = \hbar\omega(n_\beta + \frac{1}{2} + \frac{1}{2}a_\tau) - \frac{1}{4}C\beta_0^2 \quad (63)$$

with

$$a_\tau = \frac{1}{2}\sqrt{\sqrt{BC}\beta_0^4 + (2\tau + 3)^2} \quad (64)$$

For the ground state band we get

$$E^{g.s.}(\tau) = \hbar\omega\left(\frac{1}{2} + \frac{1}{2}a_\tau\right) - \frac{1}{4}C\beta_0^2 \quad (65)$$

For $\beta_0 > 0$ we expand the square root in a_τ in a Taylor-Series

$$a_\tau = \frac{1}{2}\sqrt{\sqrt{BC}\beta_0^4} \left(1 + \frac{1}{2}\frac{(2\tau + 3)^2}{\sqrt{BC}\beta_0^4} + \dots\right) \quad (66)$$

Shifting τ by

$$\tau = \hat{\tau} - 3/2 \quad (67)$$

causes the linear term to vanish and the resulting level scheme is of the form

$$E^{g.s.}(\hat{\tau}) = c_0 + c_1\hat{\tau}^2 + \dots \quad (68)$$

Therefore the γ -unstable Davidson potential is characterised by the condition, that the linear term in a shifted series expansion in τ vanishes.

In order to determine the corresponding fractional coefficient α , we shift the fractional energy spectrum by $-3/2$ and expand in a Taylor series at $J/2 = \tau = 0$ (Ψ and Ψ^1 denote the di- and trigamma function):

$$\begin{aligned} E_{\tau-\frac{3}{2}}^\alpha &= m_0 + A_0\hbar^2 \frac{\Gamma(1-\alpha/2)}{\Gamma(1-5\alpha/2)} \times \\ &\left[1 - \alpha \left(\Psi(1-5\alpha/2) - \Psi(1-\alpha/2) \right) \tau \right. \\ &+ \frac{\alpha^2}{2} \left\{ \left(\Psi(1-5\alpha/2) - \Psi(1-\alpha/2) \right)^2 \right. \\ &\left. \left. - \left(\Psi^1(1-5\alpha/2) - \Psi^1(1-\alpha/2) \right) \right\} \tau^2 + \dots \right] \end{aligned} \quad (69)$$

The linear term in τ has to vanish. Therefore α is determined by the condition

$$\Psi(1-5\alpha/2) = \Psi(1-\alpha/2) \quad (70)$$

which is fulfilled for $\alpha \approx 0.66$.

Hence for a sufficiently large β_0 the ground state band spectrum of the γ -unstable Davidson potential is reproduced within the fractional symmetric rigid rotor at $\alpha \approx 2/3$.

4.4 Linear potential limit

Besides the above discussed well established three limits there exists an additional special case, which is, in a geometric picture, the linear potential model. It has first been proposed by Fortunato[26].

Although it has not been used for a description of nuclear ground state band spectra yet, it will turn out to be useful for an understanding of nuclear spectra near closed shells discussed in the following section.

The potential is of the form

$$V(\beta) = C\beta \quad (71)$$

where C (the stiffness in β -direction) is the main parameter of the model.

The level spectrum is given approximately by[26]:

$$E(n_\beta, \tau) = \frac{3}{2}C\beta_0 + (n_\beta + \frac{1}{2})\sqrt{\frac{3C}{\beta_0}} \quad (72)$$

with

$$\beta_0 = \left(2(\tau + 1)(\tau + 2)/C\right)^{1/3} \quad (73)$$

The ground state band level spectrum is given according to conditions (52) by

$$E^{g.s.}(\tau) = \frac{3}{2}C\beta_0 + \frac{1}{2}\sqrt{\frac{3C}{\beta_0}} \quad (74)$$

We therefore are able to define the relative energy levels $f(\tau)$ in units $E^{g.s.}(1) - E^{g.s.}(0)$, which are independent of parameter C .

$$f(\tau) = \frac{E^{g.s.}(\tau) - E^{g.s.}(0)}{E^{g.s.}(1) - E^{g.s.}(0)} \quad (75)$$

An expansion in a Taylor series at $\tau = 1$ yields:

$$f(\tau) = 1 + 0.895(\tau - 1) - 0.076(\tau - 1)^2 + 0.018(\tau - 1)^3 + \dots \quad (76)$$

An equivalent expression for the fractional rotational energy is given by:

$$g(\tau, \alpha) = \frac{E_{2\tau}^\alpha - E_0^\alpha}{E_2^\alpha - E_0^\alpha} \quad (77)$$

A Taylor series expansion at $\tau = 1$ followed by a comparison of the linear terms of $f(\tau)$ and $g(\tau, \alpha)$ leads to the condition

$$\frac{2\alpha\Gamma(1-\alpha)\Gamma(3\alpha)\left(2 + 3\alpha\Psi(\alpha) - \Psi(3\alpha)\right)}{\Gamma^2(1+\alpha) - \Gamma(1-\alpha)\Gamma(1+3\alpha)} = 0.895 \quad (78)$$

which is fulfilled for $\alpha \approx 0.33$. Hence below the vibrational region at $\alpha \approx 1/2$ there exists a region at $\alpha \approx 1/3$, which corresponds to the linear potential model in a geometric picture.

Summarising the results of this section, we conclude, that a change of the fractional derivative coefficient α may

be interpreted within a geometric collective model as a change of the potential energy surface.

In a generalised, unique approach the fractional symmetric rigid rotor treats rotations at $\alpha \approx 1$, the γ -unstable limit at $\alpha \approx 2/3$, vibrations at $\alpha \approx 1/2$, and the linear potential limit at $\alpha \approx 1/3$ similarly as fractional rotations. They all are included in the same symmetry group, the fractional $SO^\alpha(3)$. This is an encouraging unifying point of view and a new powerful approach for the interpretation of nuclear ground state band spectra.

5 Comparison with experimental data

In the previous section we have shown, that the rotational, vibrational and γ -unstable limit of geometric collective models are special cases of the fractional symmetric rigid rotor spectrum.

The fractional derivative coefficient α acts like an order parameter and allows a smooth transition between these idealised cases.

Of course, a smooth transition between rotational and e.g. vibrational spectra may be achieved by geometric collective models too. A typical example is the Gneuss-Greiner model [28] with a more sophisticated potential. Critical phase transitions from vibrational to rotational states have been studied for decades using e.g. coherent states formalism or within the framework of the IBA-model [29]-[32]. But in general, within these models, results may be obtained only numerically with extensive effort.

Anyhow, only very few nuclear spectra can be described accurately by one of the four limiting, idealised cases discussed in section 4.

In the following we will prove, that the full range of low energy ground state band spectra of even-even nuclei is accurately reproduced within the framework of the fractional symmetric rigid rotor model.

For a fit of the experimental spectra E_J^{exp} we will use (49)

$$E_J^\alpha = m_0 + a_0 \frac{\Gamma(1 + (J+1)\alpha)}{\Gamma(1 + (J-1)\alpha)}, \quad J = 0, 2, 4, \dots \quad (79)$$

with the slight modification, that \hbar^2 has been included in to the definition of a_0 , so that m_0 and a_0 may both be given in units of [keV].

As a first application we will analyse typical rotational, γ -unstable, vibrational and linear type spectra. In the upper row of figure 3 the energy levels of the ground state bands are plotted for ^{156}Gd , ^{196}Pt , ^{110}Cd and ^{218}Po which represent typical rotational-, γ -unstable-, vibrational and linear type spectra [33]-[36].

The fractional coefficients α , deduced from the experimental data, are remarkably close to the theoretically expected idealised limits of the fractional symmetric rigid rotor, discussed in the previous section.

Table 1. Listed are the optimum parameter sets (α , a_0 , m_0 according (79)) for the fractional symmetric rigid rotor for different nuclids. The maximum valid angular momentum J_{max} below the onset of alignment effects are given as well as the root mean square error ΔE between experimental ([33]-[55]) and fitted energies in %.

nuclid	α	$a_0[\text{keV}]$	$m_0[\text{keV}]$	J_{max}	$\Delta E[\%]$
$^{156}_{92}\text{Gd}_{64}$	0.863	31.90	-43.65	14	2.23
$^{196}_{118}\text{Pt}_{78}$	0.710	175.06	-83.69	10	0.44
$^{110}_{62}\text{Cd}_{48}$	0.570	607.91	-405.80	6	0
$^{218}_{134}\text{Po}_{84}$	0.345	1035.69	-671.03	8	0.12
$^{164}_{88}\text{Os}_{76}$	0.624	339.423	-128.448	6	0
$^{174}_{94}\text{Os}_{76}$	0.743	125.128	-39.968	10	1.35
$^{172}_{96}\text{Os}_{76}$	0.767	89.010	-23.656	8	1.21
$^{174}_{98}\text{Os}_{76}$	0.771	63.388	-17.656	24	0.73
$^{176}_{100}\text{Os}_{76}$	0.808	51.231	-23.064	18	1.22
$^{178}_{102}\text{Os}_{76}$	0.816	49.882	-22.792	14	2.16
$^{180}_{104}\text{Os}_{76}$	0.841	45.309	-18.662	12	2.50
$^{182}_{106}\text{Os}_{76}$	0.903	32.002	-7.159	10	1.29
$^{184}_{108}\text{Os}_{76}$	0.904	31.690	-12.902	14	1.39
$^{186}_{110}\text{Os}_{76}$	0.882	40.433	-19.155	14	1.82
$^{188}_{112}\text{Os}_{76}$	0.875	44.567	-14.629	12	1.58
$^{190}_{114}\text{Os}_{76}$	0.847	58.055	-17.748	12	1.34
$^{192}_{116}\text{Os}_{76}$	0.835	63.774	-15.437	12	0.71
$^{214}_{126}\text{Ra}_{88}$	-0.007	374408	-376529	8	2.53
$^{214}_{126}\text{Ra}_{88}$	0.548	344.107	305.766	24	8.27
$^{216}_{128}\text{Ra}_{88}$	0.181	3665.36	-2887.88	10	4.22
$^{218}_{130}\text{Ra}_{88}$	0.536	321.622	-160.787	30	1.25
$^{220}_{132}\text{Ra}_{88}$	0.696	83.603	-25.966	30	0.26
$^{222}_{134}\text{Ra}_{88}$	0.831	33.221	-5.67	6	0
$^{224}_{136}\text{Ra}_{88}$	0.841	27.295	-8.849	12	1.57

Table 2. Energy levels for ^{176}Os with optimum parameter set from table 1 for the fractional symmetric rigid rotor E_J^α according to (79) compared with the experimental values E_J^{exp} from [41] and relative error ΔE in % for different angular momenta J . Note that for $J > 14\hbar$ beginning microscopic alignment effects are ignored in the fractional symmetric rigid rotor model and therefore the error is increasing.

$J[\hbar]$	$E_J^\alpha[\text{keV}]$	$E_J^{exp}[\text{keV}]$	$\Delta E[\%]$
0^+	-13.1	0.0	-
2^+	144.9	135.1	-7.29
4^+	404.4	395.3	-2.31
6^+	744.8	742.3	0.33
8^+	1155.4	1157.5	0.17
10^+	1629.6	1633.8	0.25
12^+	2162.3	2167.7	0.24
14^+	2749.8	2754.6	0.17
(16^+)	3389.2	3381.4	-0.23
(18^+)	4077.8	4019.1	-1.46
(20^+)	4813.6	4683.2	-2.78
(22^+)	5594.8	5398.8	-3.63

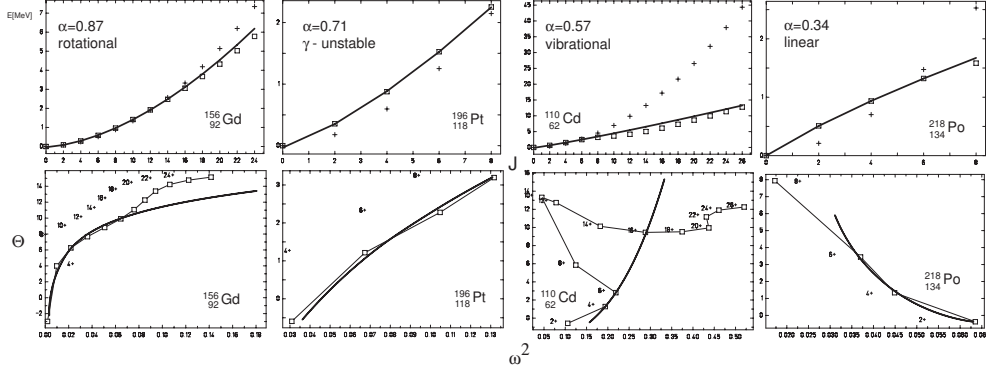


Fig. 3. The upper row shows energy levels of the ground state bands for ^{156}Gd , ^{196}Pt , ^{110}Cd and ^{218}Po are plotted for increasing J . Squares indicate the experimental values given in [33]-[36], + -symbols indicate the optimum fit of the classical symmetric rigid rotor and the curves give the best fit for the fractional symmetric rigid rotor. In the lower row the corresponding backbending plots are shown.

From the experimental data, we can roughly distinguish a rotational region for $1 \geq \alpha \geq 0.8$, a γ -unstable region for $0.8 \geq \alpha \geq 0.6$, a vibrational region for $0.6 \geq \alpha \geq 0.4$ and a linear potential region for $0.4 \geq \alpha \geq 0.2$. Experimental results are reproduced very well for all regions within the framework of the fractional symmetric rigid rotor model, while a similar fit with the classical symmetric rigid rotor gives much worse results, especially for the vibrator-like and linear spectra.

The lowering of higher angular momentum states is correctly described for rotational-, γ -unstable-, vibrational- as well as linear type spectra by the fractional symmetric rigid rotor model.

Since for higher angular momenta commencing microscopic effects limit the validity of the macroscopic fractional symmetric rigid rotor model fits, in the lower row of figure 3 the corresponding backbending plots are shown. With these plots, the maximum angular momentum J_{max} for a valid fit may be determined. In table 1 the optimum parameter sets (α, a_0, m_0) as well as the average root mean square deviation ΔE are listed. In general, the difference between experimental and calculated energies is less than 2%.

This means, that the error is better than a factor 3 to 6 compared to the results of a standard Taylor series expansion up to second order in J .

As a second application of the fractional symmetric rigid rotor, we study systematic isotopic effects for osmium isotopes [37]-[49]. Optimum fit parameter sets are given in the second part of table 1, the corresponding backbending plots are given in figure 4. In table 2 the results for the fitted ground state band energies of the fractional symmetric rigid rotor model according (79) are compared to the experimental levels [41] for ^{176}Os .

Obviously below the beginning of alignment effects the spectra are reproduced very well within the fractional symmetric rigid rotor model. The fractional coefficient α listed in table 1 increases slowly for increasing nucleon numbers. Consequently, we observe a smooth transition

of the osmium isotopes from the γ -unstable to the rotational region.

As a third application, we investigate the systematics of the ground state energy level structure near closed shells. For that purpose, in figure 5 a series of spectra of radium isotopes near the magic neutron number $N = 126$ are plotted, experimental data are taken from [50]-[55].

Starting with ^{224}Ra , the full variety of possible spectral types emerges while approaching the magic ^{214}Ra .

While ^{224}Ra and ^{222}Ra are pure rotors, ^{220}Ra shows a perfect γ -unstable type spectrum. ^{218}Ra presents a spectrum of a almost ideal vibrational type. ^{216}Ra is even closer to the magic ^{214}Ra and represents a new class of nuclear spectra.

In a geometric picture, this spectrum may be best interpreted as a linear potential spectrum as proposed in section 4.4. Typical candidates for this kind of spectrum are nuclei in close vicinity of magic numbers like $^{218}\text{Po}_{84}$, $^{154}\text{Yb}_{70}$, $^{134}\text{Xe}_{54}$, $^{96}\text{Zr}_{40}$ or $^{88}\text{Sr}_{38}$.

Finally, the experimental ground state spectrum of the magic nucleus ^{214}Ra shows a clustering of energy values: For low angular momenta α tends towards zero, which becomes manifest through almost degenerated energy levels while for higher angular momenta the spectrum tends to the vibrational type. In a classical picture this is interpreted as the dominating influence of microscopic shell effects. Within the framework of catastrophe theory [56] this observation could be interpreted as a bifurcation as well.

Therefore the fractional symmetric rigid rotor model is not well suited for a description of the full spectrum of a nucleus with magic proton or neutron numbers. But all other nuclear spectra are described with a high grade of accuracy within the framework of the fractional symmetric rigid rotor.

As a remarkable fact α reduces smoothly within the interval $1 \geq \alpha \geq 0$ while approaching a magic number, e.g. $N = 126$. Therefore, α is an appropriate order parameter for such sequences of ground state band spectra.

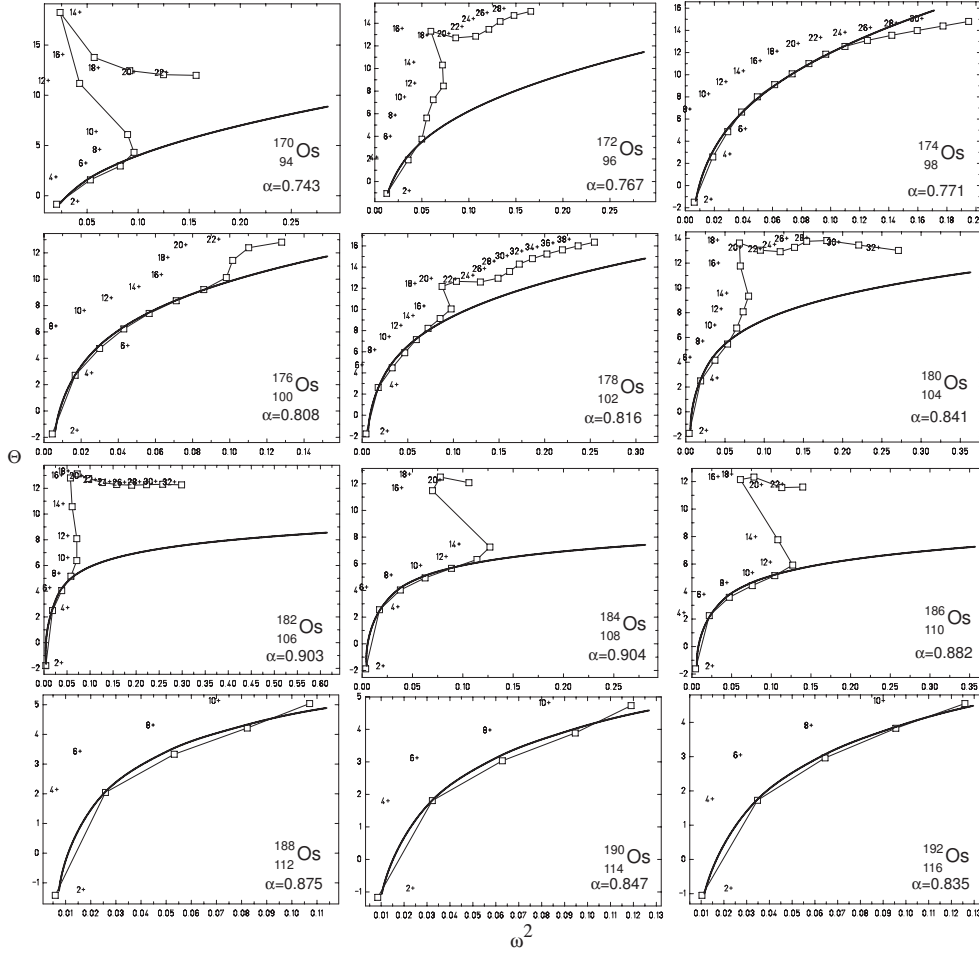


Fig. 4. For a set of osmium isotopes backbending plots are shown. Squares indicate experimental values, given in [37]–[49]. The thick line is the optimum fit result for the fractional symmetric rigid rotor. Optimum fit parameter sets are given in table 1. For the fit all angular momenta below the onset of microscopic alignment effects are included.

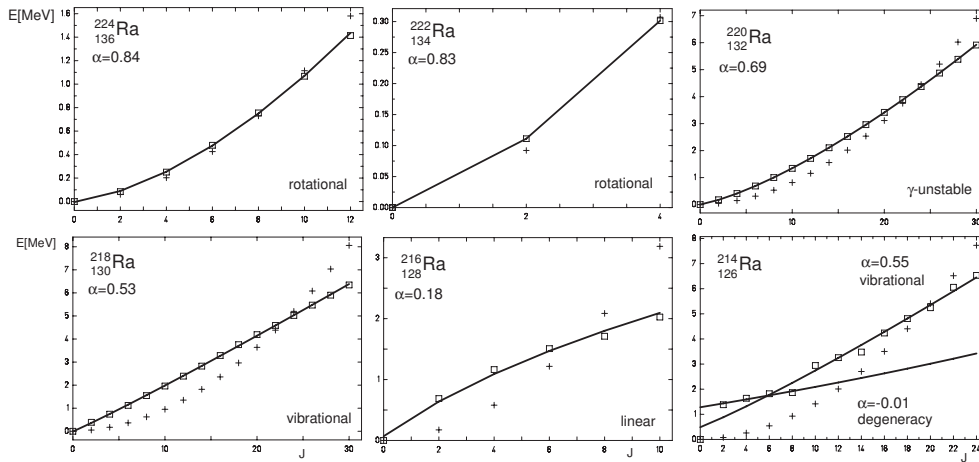


Fig. 5. The change of energy level structure of ground state bands near closed shells is illustrated for the magic neutron number $N = 126$ with a set of radium isotopes. Squares indicate experimental energy values, given in [50]–[55]. Crosses indicate the optimum fit with the standard symmetric rigid rotor model. The thick line is the optimum fit result for the fractional symmetric rigid rotor. Optimum fit parameter sets are given in the lower part of table 1. For ^{214}Ra , two different fits for low and higher angular momentum indicate the different spectral regions for magic nucleon numbers.

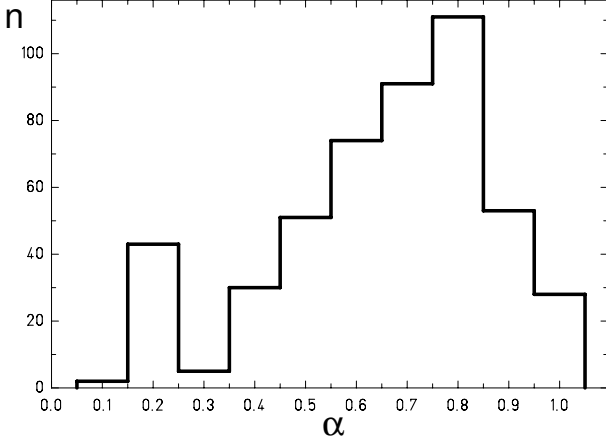


Fig. 6. The distribution $n(\alpha)$ of α -values from a fit of 490 ground state band spectra of even-even nuclei, accumulated in intervals $\Delta\alpha = 0.1$ from ${}^8\text{Be}_4$ to ${}^{256}\text{Fm}_{100}$ and ${}^{254}\text{No}_{102}$ respectively.

As a fourth application we analyse some general aspects, which are common to all even-even nuclei. Experimental ground state band spectra up to at least $J = 4^+$ are currently known for 490 even-even nuclei [57]. For these nuclei a full parameter fit according (79) was performed. The resulting distribution $n(\alpha)$ of fitted α values in 0.1 steps is plotted in figure 6.

This distribution is not evenly spread. Most of even-even nuclei exhibit rotational type ground state band spectra followed by γ -unstable and vibrational type spectra. There is a distribution gap at $\alpha \approx 0.3$. Remarkably enough, this is the region, where in a geometrical picture nuclear spectra corresponding to the linear potential model are expected.

About 8% of even-even nuclear spectra are best described with $\alpha \approx 0.2$.

The sequence of radium isotopes, presented in figure 5 reflects the general distribution of spectra for even-even nuclei.

An interesting feature may be deduced from the observation, that $n(\alpha)$ is almost linear in the region $0.3 \leq \alpha \leq 0.8$.

Hence, with the proton number Z and the neutron number N , we define the distance $R(Z, N)$ in the (Z, N) -plane, from the next magic proton or neutron number respectively to be

$$R(Z, N) = \sqrt{(Z - Z_{\text{mag}})^2 + (N - N_{\text{mag}})^2} \quad (80)$$

The linearity of $n(\alpha)$ implies a linear dependency of α on $R(Z, N)$:

$$\alpha(Z, N) = c_0 + c_1 R(Z, N) \quad , \quad 0.25 \leq \alpha \leq 0.85 \quad (81)$$

which is a helpful relation to determine an estimate of α for a series of nuclei.

Therefore the series of α values for osmium isotopes, given in table 1 may be understood even quantitatively:

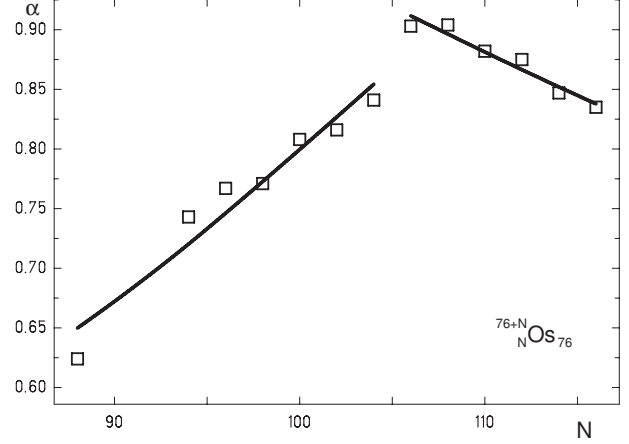


Fig. 7. Plot of fitted α parameters for a set of osmium isotopes as a function of increasing neutron number N . Squares indicate the optimum α listed in table 1. Thick lines are fits according to equation (81).

The series of ${}^{164}\text{Os}$ to ${}^{182}\text{Os}$ is closer to the $N = 82$ magic shell and therefore shows an increasing sequence in α . A least square fit yields $c_0 = 0.528$ and $c_1 = 0.0143$ with an average error in α less than 3%.

The series ${}^{184}\text{Os}$ to ${}^{192}\text{Os}$ is closer to the $N = 126$ shell and therefore shows a descending sequence in α . A least square fit yields $c_0 = 0.744$ and $c_1 = 0.008$ with an error in α less than 1%.

In figure 7 these results are presented graphically. From the figure we can deduce a prediction for $\alpha({}^{166}\text{Os}) = 0.671$ and $\alpha({}^{168}\text{Os}) = 0.695$. From these predicted α values the ratio

$$R_{4+/2+}^\alpha = \frac{E_{4+}^\alpha - E_{0+}^\alpha}{E_{2+}^\alpha - E_{0+}^\alpha} \quad (82)$$

may be deduced.

For ${}^{166}\text{Os}$ a value of $R_{4+/2+} = 2.29$ and for ${}^{168}\text{Os}$ a value of $R_{4+/2+} = 2.35$ results. These predictions are yet to be verified by experiment.

Furthermore, the sequence of osmium isotopes, presented in figure 7 indicates the position of the next magic neutron number $N = 126$. The nucleus ${}^{184}\text{Os}$ with the maximum α value in the sequence of osmium isotopes, is positioned just between the two magic numbers $N = 82$ and $N = 126$ and may be used for an estimate for the next magic neutron number.

Therefore, we propose an alternative approach to the search for super heavy elements. Instead of a direct synthesis of superheavy elements [58],[59], a systematic survey of α values of the ground state band spectra of even-even nuclei with $N > 146$ and $Z > 98$ could reveal indirect information about the next expected magic numbers $Z = 114$ and $N = 164$. The currently available experimental data do not suffice to determine these magic numbers accurately.

From the results presented we draw the conclusion, that the full variety of low energy ground state spectra of even-even nuclei is described with a high grade of accuracy

from a generalised point of view within the framework of the fractional symmetric rigid rotor.

The great advantage of the fractional symmetric rigid rotor model compared to the classical geometric models is, that nuclear ground state band spectra are described analytically with minimal effort according to equation (79) and with an excellent accuracy.

6 Conclusion

The Casimir operators and multiplets for a fractional extension of the rotation group $SO(n)$ have been classified algebraically.

The major result of a discussion of the corresponding fractional symmetric rigid rotor spectrum is, that the rotational, vibrational and so called γ -unstable limit of geometric collective models are special cases of the fractional symmetric rigid rotor spectrum. They are all treated as generalised rotations and are included in the same symmetry group, the fractional $SO^\alpha(3)$.

The fractional derivative coefficient α acts like an order parameter and allows smooth transitions between these idealised cases.

Applied to the ground state band spectra of nuclei, there is an excellent agreement with the experimental data for the full range of angular momenta up to the beginning of alignment effects. The results indicate, that the fractional symmetric rigid rotor is an appropriate tool to reproduce the low energy ground state excitation spectra of even-even nuclei.

The results encourage further studies with this model. With the knowledge of the corresponding eigenfunctions of the fractional symmetric rigid rotor e.g. a calculation of transition matrix elements was possible.

7 Acknowledgements

We thank A. Friedrich and G. Plunien from TU Dresden, Germany, for helpful discussions.

8 References

References

- Liouville J 1832 J. École Polytech., **13**, 1-162.
- Riemann B Jan 14, 1847 *Versuch einer allgemeinen Auffassung der Integration und Differentiation* in: Weber H (Ed.), *Bernhard Riemann's gesammelte mathematische Werke und wissenschaftlicher Nachlass*, Dover Publications (1953), 353.
- Miller K and Ross B 1993 *An Introduction to Fractional Calculus and Fractional Differential Equations* Wiley, New York.
- Samko S, Lebre A and Dos Santos A F (Eds.) 2003 *Factorization, Singular Operators and Related Problems, Proceedings of the Conference in Honour of Professor Georgii Litvinchuk* Springer Berlin, New York and references therein.
- Raspini A Fizika B **9**, (2000) 49.
- Raspini A Physica Scripta **64**, (2001) 20.
- Laskin N Phys. Rev. E. **66**, (2002) 056108.
- Baleanu D and Muslih S Physica Scripta **72**, (2005) 119.
- Dirac P A M 1930 *The Principles of Quantum Mechanics* The Clarendon Press, Oxford.
- Messiah A 1968 *Quantum Mechanics* John Wiley & Sons, North-Holland Pub. Co., New York.
- Caputo M Geophys. J. R. Astr. Soc. **13**, (1967) 529.
- Weyl H Vierteljahresschrift der Naturforschenden Gesellschaft in Zürich **62**, (1917) 296.
- Riesz M Acta Math. **81**, (1949) 1.
- Grünwald A K Z. angew. Math. und Physik **12**, (1867) 441.
- Podlubny I 1999 *Fractional Differential equations*, Academic Press, New York.
- Oldham K B and Spanier J 2006 *The Fractional Calculus*, Dover Publications, Mineola, New York.
- Euler L Commentarii academiae scientiarum Petropolitanae **5**, (1738) pp. 36-57.
- Louck J D and Galbraith H W Rev.Mod.Phys. **44**(3), (1972) 540.
- Greiner W and Müller B 1994 *Quantum Mechanics - Symmetries*, exercise 3.18., Springer, Berlin, Heidelberg, New York.
- Edmonds A R 1957 *Angular Momentum in Quantum Mechanics*, Princeton University Press, New Jersey.
- Rose M E 1995 *Elementary Theory of Angular Momentum*, Dover Publications, New York.
- Bohr A Mat. Fys. Medd. Dan. Vid. Selsk **26**, (1952) 14.
- Eisenberg J M and Greiner W, 1987 *Nuclear Models* North Holland, Amsterdam.
- Bohr A, *Rotational States in Atomic Nuclei* (Thesis, Copenhagen 1954).
- Davidson P M Proc. R. Soc. **135**, (1932) 459.
- Fortunato L Eur. Phys. J. A **26** s01, (2005) 1.
- Abramowitz M and Stegun I A 1965 *Handbook of mathematical functions* Dover Publications, New York.
- Gneuss G and Greiner W Nucl.Phys.A **171**, (1971) 449.
- Casten R F, Zamfir N V and Brenner D S Phys. Rev. Lett. **71**, (1993) 227.
- Feng D H, Gilmore R and Deans S R Phys. Rev. C **23**, (1981) 1254.
- Haapakoski P, Honkaranta P and Lipas P O Phys. Lett. B **31**, (1970) 493.
- Raduta A A, Gheorghe A C and Faessler A J. Phys. G **31**, (2005) 337.
- Reich C W Nuclear Data Sheets **99**, (2003) 753.
- Chunmei Z, Gongqing W and Zhenlan T Nuclear Data Sheets **83**, (1998) 145.
- Frenne D and Jacobs E Nuclear Data Sheets **89**, (2000) 481.
- Singh B Nuclear Data Sheets **107**, (2006) 1027.
- Balraj S Nuclear Data Sheets **93**, (2001) 243.
- Baglin C M Nuclear Data Sheets **96**, (2002) 611.
- Singh B Nuclear Data Sheets **75**, (1995) 199.
- Browne E and Junde H Nuclear Data Sheets **87**, (1999) 15.
- Basunia M S Nuclear Data Sheets **107**, (2006) 791.
- Browne E Nuclear Data Sheets **72**, (1994) 221.
- Wu S and Niu H Nuclear Data Sheets **100**, (2003) 483.
- Singh B and Firestone R B Nuclear Data Sheets **74**, (1995) 383.
- Firestone R B Nuclear Data Sheets **58**, (1989) 243.

46. Baglin C M Nuclear Data Sheets **99**, (2003) 1.
47. Balray S Nuclear Data Sheets **95**, (2002) 387.
48. Balray S Nuclear Data Sheets **99**, (2003) 275.
49. Baglin C M Nuclear Data Sheets **84**, (1998) 717.
50. Akovali Y A Nuclear Data Sheets **76**, (1995) 127.
51. Artna-Cohen A Nuclear Data Sheets **80**, (1997) 157.
52. Jain A K and Singh B Nuclear Data Sheets **107**, (2006) 1027.
53. Artna-Cohen A Nuclear Data Sheets **80**, (1997) 187.
54. Akovali Y A Nuclear Data Sheets **77**, (1996) 271.
55. Artna-Cohen A Nuclear Data Sheets **80**, (1997) 227.
56. Arnold V I 1992 *Catastrophe Theory* 3rd ed. Springer, Berlin.
57. see Nuclear Data Sheets and references therein
58. Oganessian Yu Ts, Utyonkov V K, Lobanov Yu V, Abdullin F Sh, Polyakov A N, Shirokovsky I V, Tsyganov Yu S, Gulbekian G G, Bogomolov S L, Gikal B N, Mezentsev A N, Iliev S, Subbotin V G, Sukhov A M, Voinov A A, Buklanov G V, Subotic K, Zagrebaev V I and Itkis M G Phys. Rev. C **69**, (2004) 054607.
59. Hofmann S, Ackermann D, Antalic S, Burkhard H G, Dressler R, Heberger F P, Kindler B, Kojouharov I, Kusunniemi P, Leino M, Lommel B, Mann R, Münzenberg G, Nishio K, Popeko A G, Saro S, Schött H J, Streicher B, Sulignano B, Uusitalo J and Yeremin A V Journal of Nuclear and Radiochemical Sciences, Vol. 7, No.1, (2006) R25

